Multifilamentation transmission through fog

G. Méjean, J. Kasparian,* J. Yu, E. Salmon, S. Frey, and J.-P. Wolf
Teramobile, LASIM, UMR CNRS 5579, Université Claude Bernard Lyon 1, 43 bd du 11 Novembre 1918, F-69622 Villeurbanne Cedex, France

S. Skupin,† A. Vinçotte, R. Nuter, S. Champeaux, and L. Bergé
Département de Physique Théorique et Appliquée, CEA/DAM Ile de France, B.P. 12, 91680 Bruyères-le-Châtel, France
(Received 11 April 2005; revised manuscript received 15 June 2005; published 19 August 2005)

The influence of atmospheric aerosols on the filamentation patterns created by TW laser beams over 10 m propagation scales is investigated, both experimentally and numerically. From the experimental point of view, it is shown that dense fogs dissipate quasi-linearly the energy in the beam envelope and diminish the number of filaments in proportion. This number is strongly dependent on the power content of the beam. The power per filament is evaluated to about 5 critical powers for self-focusing in air. From the theoretical point of view, numerical computations confirm that a dense fog composed of micrometric droplets acts like a linear dissipator of the wave envelope. Beams subject to linear damping or to collisions with randomly-distributed opaque droplets are compared.

DOI: 10.1103/PhysRevE.72.026611 PACS number(s): 42.68.Ay, 42.68.Ge

I. INTRODUCTION

High-power, ultrashort (femtosecond) laser pulses can propagate in air within a self-guided mode. This regime is often referred to as "filamentation" [1]. It requires that the beam power exceeds a critical power $P_{cr}=3.7\lambda_0^2/8\pi n_2$, where n_2 denotes the nonlinear Kerr index coefficient of dioxygen molecules and λ_0 the central laser wavelength ($P_{cr} \simeq 3$ GW at $\lambda_0=800$ nm with $n_2 \sim 3\times 10^{-19}$ cm^2/W). This condition allows Kerr-lens self-focusing to overcome diffraction. For beam powers widely above P_{cr}, several filaments with about 150 μm in diameter, forming localized structures inside the transverse beam pattern, are nucleated and can propagate over distances much longer than the Rayleigh length, from several hundreds of meters [2] up to the kilometer range [3,4]. Their very high, quasiconstant intensity lying in the order of 10^{14} W/cm^2 [5,6] allows efficient self-phase modulation and generation of a broadband white-light continuum spanning from the ultraviolet [7] to the mid-infrared[8]. Ionization of air molecules [2,9–12] in the vicinity of the filaments crucially contributes to their self-guiding, as the resulting electron plasma defocuses the pulse and keeps up a dynamic balance with the Kerr focusing response of the medium.

The main properties of the filaments (white-light generation, air conductivity, and high intensities at remote distances) open exciting ways for atmospheric applications [13]. The broad white-light continuum allows to extend the Lidar (light detection and ranging) technique with nonlinear and multispectral measurements [3,14–16]. The continuously ionized plasma channels generated in the filaments are also suitable for high-voltage discharge switching and guiding, opening the perspective for laser lightning control [17–20]. Finally, the ability of filaments to deliver high intensities at long distances permits remote elemental analysis by laser-induced breakdown spectroscopy techniques [21].

The above open-field applications stimulate the need for a better knowledge of the filament propagation in perturbed atmospheres, such as adverse weather, and especially through clouds and rain. Recent results on laboratory scales, both experimental [22] and theoretical [23,24], have shown that single filaments can survive their interaction with obscurants of diameters up to $\sim$100 μm, comparable with the filament size. They have also shown that the filamentation of a GW beam can survive the transmission through a cloud with an optical thickness as high as 3, corresponding to 5% transmission. Filament robustness is due to the refocusing of some beam components that are kept untouched after the collision and whose power remains above critical. These components again self-focus onto the beam axis and replenish the filament within a few cm. In connection with this aspect, the role of elastic losses inside the overall beam envelope (i.e., the whole focal spot playing the role of an "energy reservoir" or "photon bath" for the enclosed filaments) is crucial for maintaining the filamentary dynamics over longer distances. In Refs. [25,26], high-power beams were shown to freely propagate through long-range clusters of filaments (so-called "optical pillars") created from the initial fluctuations of the beam. Such clusters are capable of covering several tens of meters, while their constituent filaments appear and disappear recurrently over $\sim$1 m by exchanging energy with the surrounding photon bath, in agreement with the scenario proposed in Ref. [27]. In the presence of water droplets, the survival of multiple filaments has been observed qualitatively. The propagation through 5 m of a water cloud with 0.3 droplets/cm^3 having a mean diameter of 0.5 mm reduces only slightly the efficiency of a $\sim$1.5 TW beam to trigger and guide high-voltage discharges [20]. However, neither systematic experimental data nor numerical simula-

*Electronic address: jkaspari@lasim.univ-lyon1.fr
†Also at: Institute for Condensed Matter Theory and Solid State Optics, Friedrich-Schiller-Universität Jena, Max-Wien-Platz 1, 07743 Jena, Germany

tions are available to date concerning the multifilamentation of TW-class beams propagating in clouds or rain over propagation scales relevant for atmospheric applications.

In this work, we investigate for the first time the influence of a 10 m long fog on multifilamenting TW beams that propagate upon 50 m. Section II presents the experimental setup and main observations. Section III is devoted to numerical computations performed in this field.

II. EXPERIMENTAL RESULTS

A. Experimental setup

The experiments were conducted with the mobile femtosecond-Terawatt "*Teramobile*" laser system [28], allowing for outdoor experiments under any weather condition. The Teramobile produces 220 mJ pulses at 10 Hz repetition rate, centered at 800 nm. The beam is emitted in collimated geometry, with an initial diameter of 3 cm. The minimum pulse duration is 80 fs, although a chirp enlarging it up to 1 ps can be applied, in order to precompensate for group velocity dispersion (GVD) in air. In that case, the pulses are refocused temporally after a given propagation distance [29,30].

The *Teramobile* beam was propagated horizontally at the sea level (Lyon, 170 m altitude). After 40 m of free propagation, it hit a synthetic fog of water droplets produced in an open cloud chamber, already depicted in Ref. [16]. The initial laser chirp was adjusted, so that filamentation began shortly before the beam enters the cloud. This corresponds to an initial pulse duration of 600 fs. Then, the filaments propagated over 10 meters through a quasihomogeneous cloud. The cloud density was estimated by measuring the elastic transmission of a low-power He:Ne laser. Its droplet size distribution was centered at 1 μm radius (i.e., much smaller than the filament size), as monitored by using an optical sizer (Grimm model G 1-108).

Propagation in cloudy atmosphere was characterized by recording beam profiles. These were acquired by taking photographs of the beam imaged on a screen, using a digital camera. The exposure time of 1/8 s was chosen to assure that each picture corresponds to a single-shot picture. Images have been taken both over the whole spectrum, with high sensitivity to the white-light continuum and to the conical emission, and in the infrared (fundamental) region of the spectrum, yielding a good approximation of the beam profile at the considered distance, as demonstrated in Refs. [25,26].

B. Results and discussion

In a first series of experiments, we analyzed the beam pattern at the exit of the cloud chamber for high droplet densities (not shown here). The minimal input power required for observing transmission of light by one filament at the chamber exit was about 28 GW, i.e., close to $9P_{cr}$. At higher powers, filaments were clearly transmitted through the cloud and the transmitted beam energy lied above 25 mJ (power $\sim$45 GW). For a cloud length of 10 m crossed by pulses with 220 mJ incident energy, this corresponds to 12% transmission, i.e., a dense fog with an extinction coefficient of $\epsilon \simeq 0.21$ m^{-1}. Thus, filamentation can survive the propagation in a fog over a distance comparable with the fog visibility. In the cloud, the droplet density is $N=6.7\times10^4$ cm^{-3}, so that the photon mean free path (MFP) is about 5 m. Here, MFP is the average longitudinal length L_M, along which an optical object of radius r will collide a droplet of radius R, $L_M=1/\pi(r+R)^2N$. For an optical ray, we have $r\rightarrow 0$, so that $L_M=5$ m guarantees a weak interaction of photons with droplets. In contrast, a femtosecond filament with radius $r\sim 100$ μm has a MFP of only $\sim$0.5 mm, so that one individual filament hits about 2000 particles per meter of propagation. This may possibly induce substantial damage on the filamentary structure. However, the droplet radius (1 μm) is typically 100 times smaller than the filament size. Since much larger droplets are not sufficient to block the filaments [22–24], these may not be destroyed by the cloud used in our experiment, as long as droplets have a small enough mean size. With that condition, the cloud influence can be expected to occur mainly through the energy losses escaping from the overall beam envelope.

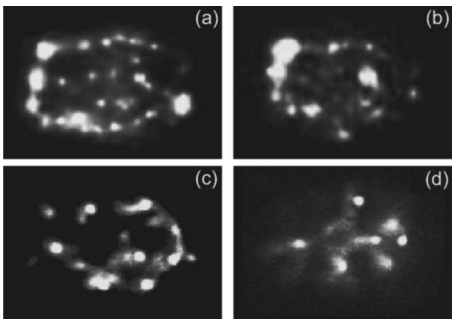

FIG. 1. Beam profiles at the exit of the 10 m long cloud chamber, in the case of both free propagation [(a) and (c)] at the respective powers of $123P_{cr}$ (220 mJ, 600 fs) and $51P_{cr}$ ($\sim$90 mJ, 600 fs), and propagation through 10 m of a dense fog [(b) and (d)] with the same powers. Subplot dimensions are about 5×3.5 cm^2.

We investigated this effect with a second series of experiments by recording beam profiles at the exit of the cloud chamber for two incident laser energies, both in the free propagation regime and with the synthetic cloud with 50% transmission. This higher transmission corresponds to an extinction coefficient of $\epsilon=0.07$ m^{-1}, i.e., to a droplet density of 2.2×10^4 cm^{-3} and a photon MFP of 14 m. As shown in Fig. 1, the transmitted beam energy strongly influences the spatial distribution of filaments, and especially their number. The filamentation patterns for close transmitted energies (90 mJ [Fig. 1(c)], and 220 mJ with 50% attenuation, i.e., 110 mJ transmitted energy [Fig. 1(b)]) indeed look similar, with most of the filaments located on a ring at the edge of the beam profile, and several of them arising inside this ring. Only a few filamentary sites have disappeared along the optical path through the fog [see Figs. 1(a)–1(d)]. The number of filaments decreases accordingly with the power left at the output of the cloud chamber. This shows that the cloud globally acts like a power attenuator on the beam as a whole. It promotes elastic extinction of the "photon bath" and its embedded filaments.

To confirm this finding, we investigated the dependency of the transmitted power on the number of filaments. It is

TABLE I. Average filament number vs input beam power after 50 m of propagation, thereof 10 m in free or foggy atmospheres.

P_{in}/P_{cr}	123		51	
Propagation	Free	Fog	Free	Fog
Filament No.	24	13	11	6

generally known that beams highly exceeding the critical power for self-focusing break up into many self-focusing cells, each containing several critical powers. Typically, the modulational instability theory predicts that about $3P_{cr}$ is engaged in each cell [31], which holds as long as a single filament experiences the surrounding background field as a uniform plane wave. For each experimental condition of Fig. 1, the filament number has been averaged over four to seven recorded profiles. Results have been summarized in Table I. Assuming weak absorption caused by plasma generation [27], the beam power transmitted over 50 m of free propagation is almost constant, whereas that crossing the cloud chamber upon the same propagation distance can be estimated by $P_{tr} \simeq P_{in}/2$. A linear fit shows in Fig. 2 a ratio of one filament cell for every 15 GW of transmitted power with $P_{cr} \simeq 3$ GW. This curve clearly indicates that about five critical powers are engaged in each filament, regardless of whether the beam propagates through a cloud or not. This estimate is in reasonably good agreement with previous expectations. It lies between the theoretical evaluations applying to purely Kerr media ($P_{fil} \sim 3P_{cr}$) [31] and recent (3+1)-dimensional simulations of femtosecond filaments self-channeling in air ($P_{fil} \sim 7P_{cr}$) [24].

Furthermore, besides energy losses, the cloud may reduce the peak power by increasing the pulse duration, because of multiple scattering. We estimated this effect by means of ray-tracing techniques and Monte Carlo simulations. Multiple scattering induced by 1 μm large droplets results in random trajectories, modeled as successive segments, whose length is the photon MFP deflected by a small angle with respect to the beam propagation axis. Differences in the trajectory lengths of rays remaining near axis at the exit of the cloud chamber yield a direct information on the modal (temporal) dispersion produced by the droplets. The rays scattered out of the beam axis are considered as lost and are discarded by the calculation. With a cloud transmission of 50%, the pulse stretching is around 100 fs, negligible for the 600 fs pulse used in the present experiment. However, at the filamentation threshold (12% transmission), the broadening is in the order of 500 fs, thus doubling the effective pulse duration. The effect would be even stronger in the case of shorter incident pulses. This semiqualitative argument indicates that the cloud affects the filamentation by reducing the laser power together with the beam energy.

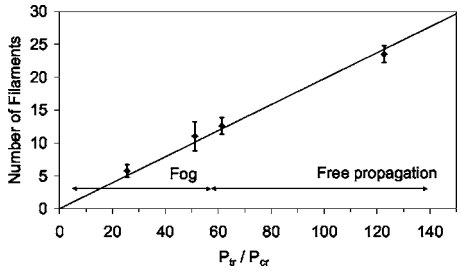

FIG. 2. Dependence of the transmitted power (P_{tr}) on the filament number for free or humid propagation [$P_{cr} \simeq 3$ GW].

III. NUMERICAL ANALYSIS

The extinction of filaments through a dense cloud is now numerically investigated. Our physical model, which captures the essential features of long-distance propagation in air, has been described in Refs. [25,26]. Originally derived in (3+1) dimensions, it consists of an extended nonlinear Schrödinger equation for the laser electric field envelope $\mathcal{E}$, coupled with a Drude model describing the growth of free electron density. These equations apply to pulses moving in their group-velocity frame, and characterized by a beam waist w_0, half-width duration t_p and central wave number $k_0 = 2\pi/\lambda_0$. They include effects of transverse diffraction, self-focusing, stimulated Raman scattering, plasma gain and losses that are mainly induced by multiphoton ionization (MPI) of dioxygen molecules.

Because experiments involve broad beams with cm waists, direct simulations in (3+1)-dimensional geometry are costly in computation time and require Terabyte storage systems when propagating the entire pulse over several tens of meters. Moreover, simulating collisions with micrometric droplets become even impossible to deal with, since the requested spatial resolution should typically access the tenth of micron for a numerical box close to 6×6 cm^2. Therefore, the present issue will be addressed in the framework of a reduced (2+1)-dimensional model, which freezes the temporal dependencies of $\mathcal{E}$. After substituting the *ansatz* $\mathcal{E}(x,y,z,t) = \psi(x,y,z) \times e^{-[t-t_c(z)]^2/T^2}$ whose temporal extent, $T \simeq t_p/10$, is assumed constant in the filamentation regime, the model equations are averaged in time following the analytical procedure described in Ref. [25], in order to establish the equation for the spatial envelope ψ as

$$\frac{\partial \psi}{\partial z} = \frac{i}{2k_0}\nabla_\perp^2 \psi + i\alpha k_0 n_2 |\psi|^2 \psi - ik_0 \frac{n_4}{\sqrt{3}} |\psi|^4 \psi - i\gamma |\psi|^{2K} \psi - \frac{\beta^{(K)}}{2\sqrt{K}} |\psi|^{2K-2} \psi - \frac{\epsilon}{2}\psi, \quad (1)$$

with $\alpha = 1/\sqrt{8} + D/4\tau_K$, $\gamma = k_0 \sigma_K \rho_{nt} \sqrt{\pi/8K} T/2\rho_c$ and

$$D \equiv \int_{-\infty}^{+\infty} e^{(T^2/8\tau_K^2) - (u/\tau_K) - (2u^2/T^2)} \left[\mathrm{erf}\left(\frac{\sqrt{2}u}{T} - \frac{T}{\sqrt{8}\tau_K} \right) + 1 \right] du. \quad (2)$$

The function D depends on the relaxation time ($\tau_K = 70$ fs) of the Raman-delayed Kerr response and it takes the value of 44 fs (resulting $\alpha = 0.51$) for a temporal duration of $t_p \simeq 510$ fs [full width at half-maximum (FWHM) = 600 fs]. The other coefficients of Eq. (1) involve parameters appropriate to air, namely, the neutral density of dioxygen molecules $\rho_{nt} = 5.4 \times 10^{18}$ cm^{-3}, the critical plasma density at

800 nm, $\rho_c \simeq 1.8\times10^{21}$ cm^{-3}, the multiphoton absorption (MPA) coefficient $\beta^{(K)} \simeq 3.1\times10^{-98}$ cm^{2K-3}/W^{K-1}, the MPI rate $\sigma_K = 2.9\times10^{-99}$ s^{-1} cm^{2K}/W^K and number of photons $K=8$. For completeness, quintic susceptibility has been introduced with weak coefficient $n_4 = 2.5\times10^{-33}$ cm^4/W^2, which was justified by recent studies [32,33]. The damping term with coefficient ϵ (in m^{-1}) describes the linear extinction of power in a beam propagating through the cloud chamber. We recall that Eq. (1) restores quantitative features in the long-range evolution of TW filamentation patterns issued from realistic broad beams [25,26]. It is, however, constrained to the approximation limiting the temporal pulse profile to one narrow time slice ($T=0.1t_p$) and cannot account for, e.g., the variations of the nonlinear focus caused by the introduction of a temporally chirped phase [30].

A. Filament decay by linear damping and random collisions with obscurants

We examine the changes occurring in filamentation patterns caused either by a linear damping or by collisions with droplets randomly distributed in the (x,y) plane. Such collisions are currently modeled by means of the Mie theory [34] for light scattering by spheres. Since Mie scattering is almost independent of the optical properties of the scatterers, it is possible to model droplets by opaque screens of suitable size in the simulations. This property was exploited in Ref. [24], where droplets were numerically designed as a circular amplitude mask with radius R and maximum opacity (zero transmission) at their center (x_0,y_0). This modeling provides good results for the interaction of one filament with a single droplet. For example, simulations proved that a single filament self-heals over only 2 cm of propagation with an energy loss limited to around 10%, which agrees with the experimental observations of Ref. [22]. This property, however, does not guarantee that many filaments can survive sharp interactions with thousands of small obscurants placed upon a long optical path.

To address this point, we first integrate Eq. (1) for a mm-waisted Gaussian beam ($w_0=2$ mm) having a FWHM duration of 600 fs and ~110 critical powers perturbed by a 20% random noise. On the one hand, we let the beam propagate freely over 1 m, before it reaches a 10 m long zone in which linear dissipation becomes active with $\epsilon=0.07$ m^{-1}. This value insures in principle an attenuation rate of 50% over 10 m. On the other hand, we impose $\epsilon=0$, but model the random collisions of the beam with the micrometric obstacles used in Ref. [24]. In this case, a random number of droplets located at random positions is computed at each z step. These positions are assumed to be uniformly distributed with respect to x and y. Hence, for each droplet we generate two random numbers between −0.5 and 0.5 and multiply them by L_x and L_y, that denote the sizes of the computation window. Since the number of droplets in one z step is small compared to their total number, a Poisson statistics may be used. We fix the expected average number of droplets at a z step, Δz, by $\lambda=\Delta z L_x L_y N$, where N is the droplet density. Then, the Poisson density function $\mathcal{P}(l)=\lambda^l/l!\times\exp(-\lambda)$ gives the probability to find exactly l droplets between z and $z+\Delta z$. The number l is computed from the Poisson distribution function $\mathcal{F}_{\mathcal{P}}(l)=\Sigma_{l'=0}^{l}\mathcal{P}(l')$ by means of the standard probability theory. Following this procedure, the average droplet number λ is linked to the dissipation parameter ϵ, when we specify the average relative loss induced by a single droplet. Assuming that droplets do not overlap, the rate of losses caused by the obstacles along one z step can be evaluated by $\lambda\pi R^2/L_xL_y$. Besides, the equivalent loss rate induced by the extinction coefficient ϵ is $\epsilon\Delta z$, since $\exp(-\epsilon\Delta z)\simeq 1-\epsilon\Delta z$. Identifying both contributions leads to $\epsilon=N\pi R^2$, which agrees with the experimental estimates for ϵ, N and R given in Sec. II.

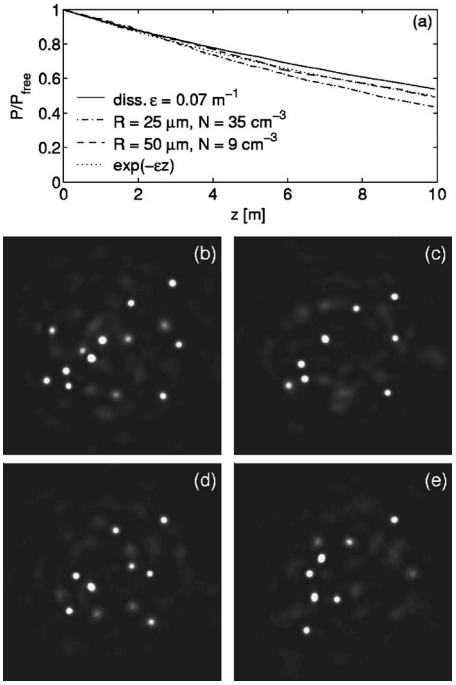

FIG. 3. (a) Numerically computed beam power scaled by the power of a freely propagating narrow beam ($w_0=2$ mm) of $\sim 110P_{cr}$ through a 10 m long fog with linear damping ($\epsilon=0.07$ m^{-1}, solid curve), random distributions of 25 μm droplets (dashed-dotted curve), and of 50 μm droplets (dashed curve). The distance $z=0$ marks the entrance into the cloud chamber. (b)–(e) Filamentation patterns at 4 m inside the cloud chamber. Subplots correspond to (b) free propagation, (c) linear damping, random droplets with radii of (d) 25 μm, and (e) 50 μm, respectively. Subplot dimensions are 7×7 mm^2. Intensity levels are twice higher than the initial intensity.

Because computer limitations prevented us from resolving obstacles of 1 micron large, we adopted the density for larger droplets with different radius $R\geqslant 25$ μm by means of the direct rescaling $N\rightarrow N/R^2[\mu\text{m}]$, in order to keep the average losses constant. Results are illustrated in Fig. 3. Figure 3(a) shows the power decrease inside the cloud chamber, normalized with respect to the power of the freely propagating beam. All curves lie closely to each other, within a margin less than ±5% around the exponential decrease $e^{-\epsilon z}$ (note that the curve for linear damping also accounts for Kerr, MPI, and MPA nonlinearities and cannot exactly fit this exponential function). This property was retrieved when using different densities N and adapted values of ϵ. Here, the decrease of

power undergone by the 2 mm beam from random collisions with droplets of 25 μm as well as 50 μm radius almost superimposes with that induced by linear dissipation over 4 m. Beam profiles at this distance are detailed in Figs. 3(b)–3(e). After only 4 m of "humid" propagation, the filamentation patterns remain similar in linearly damped regime and in the presence of random droplets ($\sim$8 cells). Compared with the free propagation regime [Fig. 3(b)], the number of filaments has already decreased by a factor $\sim 3/2$ [Figs. 3(c)–3(e)]. Analogy in the power losses and filament number between droplets of different sizes follows from the fact that, even if small droplets embark half-energy of the big ones per collision event (see, e.g., Ref. [22]), their density is four times higher and cause equivalent damage on the filamentation patterns.

At further distances ($z \rightarrow 10$ m), the filaments decrease in number, but this number is preserved with linear dissipation and random droplets (not shown here). This confirms the good agreement between the power losses induced by random collisions with micrometric obscurants and those induced by linear damping. Note, however, that the power lost from random droplets can reach $\sim$55% at large distance. Although small, these discrepancies are related to the finiteness of the numerical box, from which escaping field components increases the losses. This tendency is amplified by the opacity of the droplets, which favors large-angle diffraction to the boundaries.

In summary, droplet-induced losses are identical at constant product $N \times R^2$, i.e., they are similar for droplets with different radii, provided that the density N is tuned accordingly. They follow an exponential-like decrease comparable with the energy fall produced by a linear damping. These findings confirm the equivalence between collisions of an optical beam with randomly distributed droplets and exponential attenuation of its power.

B. Linear damping vs filamentation patterns

Because linear damping and droplet collisions induce analogous power losses, we investigate the consequences of a linear damping on broad beams inside a 10 m dense fog after a 40 m long stage of free propagation, in conditions close to the experimental setup. We enlarge the beam waist to the value $w_0 = 1$ cm, applied to a digitized file of the experimental input beam fluence. This value is willingly chosen smaller than the experimental beam waist, in order to compensate for the limitations of Eq. (1) recalled above. This model cannot indeed account for the temporal compression induced by pulse chirping (see Sec. II) and it artificially decreases the effective ratio of power over critical when imposing $T = 0.1 t_p$ (see Ref. [30]). The need to make a fully bloomed filamentation pattern emerge before the cloud chamber ($z < 40$ m) implies us to select a Rayleigh length smaller than the experimental one, which justifies the choice of $w_0 = 1$ cm. Figure 4 shows the filamentary patterns outgoing from the fog tube at $z = 50$ m, after crossing the 10 m long water cloud with 50% transmission. These patterns are in qualitatively good agreement with their experimental counterparts shown in Fig. 1. In the absence of fog, the transverse profile of the beam still contains about 25 filaments [Fig. 4(a)]. This number is almost halved when the beam undergoes linear damping [Fig. 4(b)]. The resulting number of filaments (12–15) is of the same order as that obtained over a 50 m long free propagation range, when the beam only involves an initial power divided by a factor ~ 2 [Fig. 4(c)]. The same beam with 51 critical powers undergoes a drastic reduction of filaments when it propagates through the 10 m tube with a 50% linear damping [Fig. 4(d)]. The bottom inset of this figure demonstrates that MPA losses remain weak over 50 m compared with linear damping, which supports the approximation on the transmitted power $P_{tr} \simeq P_{in}/2$ made in Sec. II. The counted filaments then correspond to the bright spots visible in Fig. 4. Their number, summarized in Table II, is in very good quantitative agreement with the data mentioned in Table I. Differences in the exact number and location of the filaments compared with the experimental profiles are attributed to the smaller beam waist and to fluctuations of secondary importance (local diffusion, atmospheric turbulence, see Ref. [26]), which we ignore.

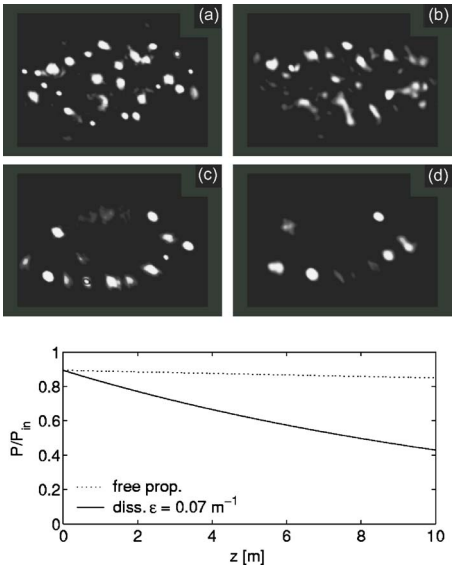

FIG. 4. Numerically computed beam profiles at the exit of the cloud chamber ($z = 50$ m), in the case of both free propagation [(a) and (c)] at the respective powers of $123 P_{cr}$ and $51 P_{cr}$ and propagation through 10 m of a dense fog [(b) and (d)] with the same powers. Window scales are 2.3×1.6 cm^2. Intensity levels correspond to twice the initial intensity. Bottom inset compares the power losses normalized to P_{in} between free propagation and linearly damped regimes for $P_{in} \simeq 123 P_{cr}$. $z = 0$ marks the entrance of the cloud chamber.

TABLE II. Filament number vs input beam power provided by numerical computations. The additional datum with 62 critical powers concerns filaments counted from the same beam in free propagation regime (not shown in Fig. 4).

P_{in}/P_{cr}	123		62	51	
Propagation	Free	Fog	Free	Free	Fog
Filament No.	25	12–15	13	12	6

These last results are instructive: They validate the experimental estimate of about 5 critical powers per filament. In free propagation regime, they also highlight the strong correlation between the number of critical powers in the starting beam and the number of filaments formed along the course of the pulse. They finally confirm again that the effect of a dense cloud enclosing sufficiently small droplets (compared with the filament size) is equivalent to a linear dissipation source acting on the energy reservoir formed by the beam envelope and its filaments.

IV. CONCLUSION

In summary, we have studied both experimentally and numerically the propagation of ultrashort laser pulses with powers much above critical in multifilamentation regimes through dense fogs. We showed that filament transmission through clouds is not restricted to the laboratory scale [22], but also occurs when multiple filaments take place over a distance comparable with the visibility length of the fog.

From the theoretical point of view, we examined differences in the transmitted light, when the model equations account for either linear damping or a stochastic hitting of the beam by micrometric obstacles. Because of computer limitations, we could not access the interaction of femtosecond pulses with 1 μm large droplets. However, our simulations revealed that randomly distributed opaque droplets with radius $\geqslant 25$ μm induce comparable energy losses, with an exponential fall. The equivalence between linear damping and losses caused by micrometric droplets enabled us to numerically reproduce the experimental filamentation patterns and achieve a very good agreement on their number of filaments.

As a conclusion, the fact that clouds do not significantly affect the filamentation process (only the number of filaments is reduced quasilinearly by power extinction) is of high interest for applications, because it implies that the filament features such as white-light generation, ionization of air or the delivery of high intensities at long distances are not forbidden inside or beyond clouds, as long as their density permits to transmit several critical powers. Therefore, the corresponding applications, respectively, multicomponent Lidar, lightning control or remote laser-induced breakdown spectroscopy (LIBS or RFIBS [20]) are still feasible within cloudy atmospheres.

ACKNOWLEDGMENTS

This work has been carried out within the framework of the Teramobile project, funded jointly by the CNRS, DFG, and French and German Ministries of Foreign Affairs. The Teramobile website is www.teramobile.org. Numerical simulations were performed on the COMPAQ alpha cluster (TERA) of CEA-France and on the IBM p690 cluster (JUMP) of the Forschungs-Zentrum in Jülich-Germany.

[1] A. Braun, G. Korn, X. Liu, D. Du, J. Squier, and G. Mourou, Opt. Lett. **20**, 73 (1995).
[2] B. La Fontaine, F. Vidal, Z. Jiang, C. Y. Chien, D. Comtois, A. Desparois, T. W. Johnston, J.-C. Kieffer, H. Pépin, and H. P. Mercure, Phys. Plasmas **6**, 1615 (1999).
[3] M. Rodriguez, R. Bourayou, G. Méjean, J. Kasparian, J. Yu, E. Salmon, A. Scholz, B. Stecklum, J. Eislöffel, U. Laux, A. P. Hatzes, R. Sauerbrey, L. Wöste, and J.-P. Wolf, Phys. Rev. E **69**, 036607 (2004).
[4] G. Méchain, A. Couairon, Y.-B. André, C. D'amico, M. Franco, B. Prade, S. Tzortzakis, A. Mysyrowicz, and R. Sauerbrey, Appl. Phys. B: Lasers Opt. **B79**, 379 (2004).
[5] J. Kasparian, R. Sauerbrey, and S. L. Chin, Appl. Phys. B: Lasers Opt. **B71**, 877 (2000).
[6] A. Becker, N. Aközbek, K. Vijayalakshmi, E. Oral, C. M. Bowden, and S. L. Chin, Appl. Phys. B: Lasers Opt. **B73**, 287 (2001).
[7] N. Aközbek, A. Iwasaki, A. Becker, M. Scalora, S. L. Chin, and C. M. Bowden, Phys. Rev. Lett. **89**, 143901 (2002).
[8] J. Kasparian, R. Sauerbrey, D. Mondelain, S. Niedermeier, J. Yu, J.-P. Wolf, Y.-B. André, M. Franco, B. Prade, A. Mysyrowicz, S. Tzortzakis, M. Rodriguez, H. Wille, and L. Wöste, Opt. Lett. **25**, 1397 (2000).
[9] H. Schillinger and R. Sauerbrey, Appl. Phys. B: Lasers Opt. **B68**, 753 (1999).
[10] S. Tzortzakis, B. Prade, M. Franco, and A. Mysyrowicz, Opt. Commun. **181**, 123 (2000).
[11] A. Talebpour, A. Abdel-Fattah, and S. L. Chin, Opt. Commun. **183**, 479 (2000).
[12] A. Talebpour, J. Yang, and S. L. Chin, Opt. Commun. **163**, 29 (1999).
[13] J. Kasparian, M. Rodriguez, G. Méjean, J. Yu, E. Salmon, H. Wille, R. Bourayou, S. Frey, Y.-B. André, A. Mysyrowicz, R. Sauerbrey, J.-P. Wolf, and L. Wöste, Science **301**, 61 (2003).
[14] P. Rairoux, H. Schillinger, S. Niedermeier, M. Rodriguez, F. Ronneberger, R. Sauerbrey, B. Stein, D. Waite, C. Wedekind, H. Wille, and L. Wöste, Appl. Phys. B: Lasers Opt. **B71**, 573 (2000).
[15] G. Méjean, J. Kasparian, E. Salmon, J. Yu, J.-P. Wolf, R. Bourayou, R. Sauerbrey, M. Rodriguez, L. Wöste, H. Lehmann, B. Stecklum, U. Laux, J. Eislöffel, A. Scholz, and A. P. Hatzes, Appl. Phys. B: Lasers Opt. **B77**, 357 (2003).
[16] G. Méjean, J. Kasparian, J. Yu, S. Frey, E. Salmon, and J.-P. Wolf, Appl. Phys. B: Lasers Opt. **B78**, 535 (2004).
[17] B. La Fontaine, D. Comtois, C. Y. Chien, A. Desparois, F. Gérin, G. Jarry, T. W. Johnston, J.-C. Kieffer, F. Martin, R. Mawassi, H. Pépin, F. A. M. Rizk, F. Vidal, C. Potvin, P. Couture, and H. P. Mercure, J. Appl. Phys. **88**, 610 (2000).
[18] B. La Fontaine, F. Vidal, D. Comtois, C. Y. Chien, A. Desparois, T. W. Johnston, J.-C. Kieffer, H. P. Mercure, H. Pépin, and F. A. M. Rizk, IEEE Trans. Plasma Sci. **27**, 688 (1999).
[19] M. Rodriguez, R. Sauerbrey, H. Wille, L. Wöste, T. Fujii, Y.-B. André, A. Mysyrowicz, L. Klingbeil, K. Rethmeier, W. Kalkner, J. Kasparian, E. Salmon, J. Yu, and J.-P. Wolf, Opt. Lett. **27**, 772 (2002).
[20] R. Ackermann, K. Stelmaszczyk, P. Rohwetter, G. Méjean, E.

Salmon, J. Yu, J. Kasparian, G. Méchain, V. Bergmann, S. Schaper, B. Weise, T. Kumm, K. Rethmeier, W. Kalkner, J.-P. Wolf, and L. Wöste, Appl. Phys. Lett. **85**, 5781 (2004).
[21] K. Stelmaszczyk, P. Rohwetter, G. Méjean, J. Yu, E. Salmon, J. Kasparian, R. Ackermann, J.-P. Wolf, and L. Wöste, Appl. Phys. Lett. **85**, 3977 (2004).
[22] F. Courvoisier, V. Boutou, J. Kasparian, E. Salmon, G. Méjean, J. Yu, and J.-P. Wolf, Appl. Phys. Lett. **83**, 213 (2003).
[23] M. Kolesik and J. V. Moloney, Opt. Lett. **29**, 590 (2004).
[24] S. Skupin, L. Bergé, U. Peschel, and F. Lederer, Phys. Rev. Lett. **93**, 023901 (2004).
[25] L. Bergé, S. Skupin, F. Lederer, G. Méjean, J. Yu, J. Kasparian, E. Salmon, J.-P. Wolf, M. Rodriguez, L. Wöste, R. Bourayou, and R. Sauerbrey, Phys. Rev. Lett. **92**, 225002 (2004).
[26] S. Skupin, L. Bergé, U. Peschel, F. Lederer, G. Méjean, J. Yu, J. Kasparian, E. Salmon, J.-P. Wolf, M. Rodriguez, L. Wöste, R. Bourayou, and R. Sauerbrey, Phys. Rev. E **70**, 046602 (2004).
[27] M. Mlejnek, M. Kolesik, J. V. Moloney, and E. M. Wright, Phys. Rev. Lett. **83**, 2938 (1999).
[28] H. Wille, M. Rodriguez, J. Kasparian, D. Mondelain, J. Yu, A. Mysyrowicz, R. Sauerbrey, J.-P. Wolf, and L. Wöste, Eur. Phys. J.: Appl. Phys. **20**, 183 (2002).
[29] J. Kasparian and J.-P. Wolf, Opt. Commun. **152**, 355 (1998).
[30] R. Nuter, S. Skupin, and L. Bergé, Opt. Lett. **30**, 917 (2005).
[31] L. Bergé, Cl. Gouédard, J. Schjødt-Eriksen, and H. Ward, Physica D **176**, 181 (2003), and references therein.
[32] A. Vinçotte and L. Bergé, Phys. Rev. A **70**, 061802(R) (2004).
[33] L. Bergé, S. Skupin, G. Méjean, J. Kasparian, J. Yu, S. Frey, E. Salmon, and J.-P. Wolf, Phys. Rev. E **71**, 016602 (2005).
[34] G. Mie, Ann. Phys. **25**, 337 (1908).